Conductance Selectivity of Na+ Across the K+ Channel via Na+ Trapped in a Tortuous Trajectory

PNAS
www.pnas.org

Main Manuscript for

Conductance Selectivity of Na^+ Across K^+ Channel via Tortuous Trajectory with Long Residency Time

Kenichiro Mita,[1,2‡] Takashi Sumikama,[1,3‡] Masayuki Iwamoto,[1,4] Yuka Matsuki,[1,2] Kenji Shigemi,[2] Shigetoshi Oiki[1,5*]

[1]Department of Molecular Physiology and Biophysics, Faculty of Medical Sciences, University of Fukui, Fukui 910-1193, Japan.

[2]Department of Anesthesiology and Reanimatology, University of Fukui, Fukui 910-1193, Japan.

[3]Nano Life Science Institute (WPI-NanoLSI), Kanazawa University, Kakuma-machi, Kanazawa 920-1192, Japan.

[4]Department of Molecular Neuroscience, Faculty of Medical Sciences, University of Fukui, Fukui 910-1193, Japan.

[5]Biomedical Imaging Research Center, University of Fukui, Fukui 910-1193, Japan.

* Shigetoshi Oiki

Email: oiki-fki@umin.ac.jp

0000-0002-8438-6750

Classification

Biological Sciences, Physiology.

Keywords

selectivity filter, single-channel current, MD simulation, single-channel conductance ratio, large-pass filter.

Author Contributions

SO designed the study. KM wrote the initial draft of the manuscript. KM, TS, MI, and SO contributed to the analysis and interpretation of data. All the other authors have contributed to data collection and interpretation and critically reviewed the manuscript. All authors approved the final version of the manuscript. ‡These authors contributed equally

This PDF file includes:

Main Text
Figures 1 to 6

Abstract

Ion selectivity of the potassium channel is crucial for regulating electrical activity in all living cells, but the mechanism underlying ion selectivity of the potassium channel that favors large K^+ ions over small Na^+ ions remains unclear. Generally, Na^+ is not completely excluded from permeation through potassium channels. Herein, the distinct nature of Na^+ conduction through the prototypical KcsA potassium channel was examined using single-channel current recordings and molecular dynamics simulations. At a high Na^+ concentration (200 mM), the channel was blocked by Na^+, which was relieved at high membrane potentials, suggesting passage of Na^+ across the channel. At 2000 mM Na^+ concentration, the single-channel Na^+ conductance was measured as one-eightieth of the K^+ conductance, indicating that the selectivity filter allows substantial conduit of Na^+. Molecular dynamics simulations revealed the unprecedented atomic trajectories of Na^+ permeation. In the selectivity filter having a series of carbonyl-oxygen rings, we found that a smaller Na^+ ion was distributed off-center in eight-carbonyl oxygen-coordinated sites as well as on-center in four-carbonyl oxygen-coordinated sites. This amphipathic nature of Na^+ coordination yielded a continuous but tortuous path along the filter, rather than the straight path for K^+. Multiple Na^+ ions in the filter took more degrees of freedom in their configurations. Accordingly, the residency time of Na^+ was much longer than that of K^+, leading to slow elution via their tortuous trajectories. The kinetic differentiation along the filter underlies the conductance selectivity which poses a basis for understanding the selectivity mechanism of numerous ion channels.

Significance Statement

Ion selectivity is a fundamental property of the ion channels, and potassium channels exhibit a distinct selectivity, allowing the passage of large K^+ ions (ionic radius of 1.3 Å) over that of smaller Na^+ ions (1.0 Å). The mechanism underlying the large-pass selectivity remains unknown. Here, we applied Na^+ as a probe for the selectivity mechanism and revealed small conduction of Na^+ across the prototypical potassium channel. In the selectivity filter, low permeable Na^+ exhibited a tortuous trajectory while highly permeable K^+ took a straight pass. Multiple Na^+ ions occupy the tortuous path more tightly than that of K^+, rendering Na^+ slowly eluted across the pore. The structure of the selectivity filter serves differential paths for different sized ion species.

Main Text

Introduction

Ion selectivity is a fundamental property of the ion channels that generate physiological functions of the cell membrane. The ion selectivity determines the direction of net currents through a channel under given ionic compositions of intracellular and extracellular solutions (1). The

potassium channels carry outward K^+ currents even in the presence of abundant Na^+ ions in the extracellular solution by allowing the passage of large K^+ ions (ionic radius of 1.3 Å) over that of smaller Na^+ ions (1.0 Å)(2–5). This is a distinct nature of potassium channel selectivity amongst other channels. The molecular mechanisms underlying this selectivity have been studied extensively for decades (2, 4, 6–8) but remain to be elucidated (6, 9–11). To examine the selectivity mechanism, the KcsA potassium channel has been applied as a prototypical channel, for which a broad spectrum of data related to ion permeation and selectivity has been accumulated (8, 12–17). The crystal structure of the KcsA channel revealed that the selectivity filter is narrow (3 Å in diameter) and short (12 Å in length), which is common for all potassium channels.

Generally, potassium channels share a typical selectivity feature for monovalent cations, and the permeability ratio relative to K^+, which is the most frequently used parameter for the ion selectivity, is plotted here as a function of the ionic radius of the relevant ion species (Fig. 1)(1, 4). The channel allows the permeation of ionic species in a limited window with respect to the ion size. Ionic species with ionic radii ranging from 0.9 to 1.7 Å, including K^+, Tl^+, Rb^+, and Na^+ as a limiting case, are permissible for conduction; however, larger and even a smaller ion (Li^+) are rejected from permeation. This feature has been explained by the classical and static concept of the snug fit (3, 18), wherein ion species within a limited ion size are selected by matching them to the cavity size in the pore. However, the molecular dynamics (MD) simulation has demonstrated that the filter structure is intrinsically flexible, dismissing the strict cavity size (14). Moreover, the crystal structure revealed that even the non-conducting Li^+ ion is bound in the selectivity filter (12). A more dynamic picture of the cavity, such as with the concept of strain energy, was proposed (10, 14, 19).

In the selectivity filter, K^+ is coordinated to eight carbonyl oxygens (cage configuration), whereas Na^+ is coordinated to four carbonyl oxygens (plane configuration) (9, 12, 20–24). The high-affinity K^+ binding to the filter deduced from the equilibrium crystal structure and spectroscopy has been interpreted as the basis for the strict K^+ selectivity (25–28). However, a comparison between the affinity and the conductance revealed that the high affinity of each ion is not a determinant of the selectivity (11, 29). Recently, data supporting low-affinity bindings of K^+ to the filter have been accumulated (30–32), and a dynamic principle for the selectivity has been proposed as an alternative mechanism. Accordingly, the tactical ion selection of potassium channels has been attributed to multiple principles underlying binding to a few specific sites (10, 33, 34). However, the distinct nature of Na^+ relative to that of K^+ under the collective dynamics of ions and water within the selectivity filter remain elusive (9, 12, 20, 21, 33, 35–37) (see references in the following review articles (6, 9–11, 33, 35)).

Here we consider that the selectivity arises dynamically and traveling ions undergo multiple selection steps, each step with different principles, along the passage of the entire pore. To decompose these selectivity processes, we describe the unique selectivity of the potassium channels as a feature of a band-pass filter with respect to the ion size (broken green line, Fig. 1). Generally, a band-pass filter is fabricated from a combination of low- and high-pass filters(38). Accordingly, the band-pass feature of the ion selectivity can be deconvoluted into two types of successive filtering processes along the pore. As a small-pass (low-pass) filter (broken blue line, Fig. 1), the potassium channels allow the passage of small ionic species with a size cut-off of ~1.7 Å; the working principle of the small-pass filter is shared with that of other types of channels, and is determined by the geometrical pore size (1, 39). Simultaneously, the potassium channels impose a unique large-pass (high-pass) filter (broken red line, Fig. 1), which rejects small ions; this is the main issue addressed and studied herein.

Na^+ is a small ion serving as a signature ion to characterize the conduction features through the potassium channels; consequently, in this study, Na^+ conduction was examined using single-channel current recordings and MD simulations for the KcsA potassium channel. To characterize the selectivity, the permeability ratio from experimentally measured reversal potentials has frequently been used, as in Fig. 1. Although it is an experimentally feasible parameter, the underlying Nernst-Planck equation assumes independent ion diffusion across a homogeneous membrane phase, rather than through a structured pore (1, 40). The reversal potential for

calculating the permeability ratio is simply the membrane potential at which inward currents and outward currents are balanced (zero-current potential). Alternatively, the single-channel conductance ratio at a specific membrane potential for different ion species is more straightforward, contrasting the integrated permeation kinetics of different ion species through the pore (4). However, it has not frequently been obtained (12, 20, 35) because of experimental difficulty. The single-channel conductance of Na^+ through the potassium channel has not been measured experimentally, although indirect evidence of Na^+ conduction through a potassium channel in the single-channel level has been reported as punchthrough (12, 13). In this study, intracellular Na^+ concentration was increased, exceeding the physiological concentration range, and the distinct Na^+ processes in the pore were resolved, which involved blocking and a single-channel Na^+ current through the potassium channel. MD simulations revealed the unprecedented conduction processes of Na^+ at an atomic scale across the channel. Accordingly, critical permeation processes involved in the large-pass filter for Na^+ conduction have been highlighted here.

Results

Single-channel behavior of E71A mutant channel under bi-ionic conditions

Single-channel current of the KcsA channel in the presence of Na^+ in the intracellular solution was examined. The KcsA potassium channel was reconstituted into the lipid bilayer using the contact bubble bilayer method (41–43). The acidic pH of one of the compartments (intracellular side) allowed measurements of functionally oriented channels (see Materials and Methods). Experiments were performed using a Na^+ solution (200 mM) with no other cations in the intracellular side. The presence of K^+ ions in the extracellular side (200 mM) allowed the detection of the single-channel current at negative membrane potentials. Throughout the study, the non-inactivating E71A mutant of the KcsA channel was adopted for elucidating Na^+ permeation through the open filter structure, and all experiments were performed under single-channel current-resolvable conditions to exclude the anomalous E71A channel activity (13).

An outward current carried by Na^+ at +200 mV is not detected (Fig. 2Ab). In a reference experiment with the pure K^+ ions contained in both the intracellular and extracellular solutions (200 mM; Fig. 2Aa), signature single-channel currents of the E71A-mutant KcsA channel (nearly 100% open probability under all voltages and flicker currents at negative potentials) are observed. Similar to those for Na^+, outward currents are not detected for Li^+ and N-methyl-D-glucamine ($NMDG^+$)(Fig. 2Ac–d).

For the $[NMDG^+]_i/[K^+]_o$ solution (i: inner solution, o: outer solution), an inward K^+ current similar to that noted for the symmetric K^+ solution was observed when the membrane potential was turned negative (−100 mV, Fig. 2Ad). In contrast, in $[Li^+]_i/[K^+]_o$ and $[Na^+]_i/[K^+]_o$ solutions, the channel opens after a delay with a negative jump (Fig. 2 Ab,c red arrows). This result indicates that Li^+ and Na^+, but not $NMDG^+$, enter the pore at positive potentials; they are then released back to the intracellular solution from the pore after a delay at a negative potential. This behavior represents a typical slow blocking such that Na^+ and Li^+ ions travel halfway through the pore into the filter, where they are trapped until delayed release occurs at the negative potential. The delay time for the opening at negative potentials indicates a high energy barrier for returning to the conductive state. This slow blocking is observed when the membrane potential is above +100 mV.

The blocking time was examined using similar pulse protocols with incremental pulse duration and determined as 147.1 $\pm$ 21.8 ms (n = 3 - 16) at +200 mV (Fig. S1). For unblocking at negative potentials, the unblocking time was obtained by ensemble averaging the current traces (Fig. S2). This behavior is typical for channel blocking, and the time constants of blocking and unblocking were in the range of ~100 ms for both Na^+ (unblocking time constant at –200 mV = 165.6 $\pm$ 33.5 ms, n = 5) and Li^+ (blocking time constant at +200 mV = 112.7 $\pm$ 36.3 ms, n = 4 – 27, and the unblocking time constant at – 200 mV = 324.2 $\pm$ 32.5 ms, n = 11). Accordingly, at low positive potentials below +100 mV, Na^+ and Li^+ are effectively excluded from entering the filter, but they

remain blocked once they entered the filter at high potentials until intracellular release at negative potentials. This process is schematically illustrated as solid blue arrows (Fig. 2E).

Invisible Na^+ conduction across the channel

The slow blocking for Na^+ and Li^+ at positive potentials is invisible, but the blocking probability is evaluated from the delayed opening at negative potentials (Fig. 2B). To attain steady-state blocking, the duration of the positive pulse was set to 1 s, which is much longer than the blocking time (Fig. S1). Upon the negative jump to −100 mV, a few channels in the membrane are opened successively with distinct delay times in $[Na^+]_i/[K^+]_o$ (Fig. 2Ba) and $[Li^+]_i/[K^+]_o$ (Fig. 2Bb) solutions. The number of open channels at the beginning of the negative potential jump provides a rough estimate of the blocked probability at the positive potential (P_{block}). Ensemble averaging of the single-channel current traces was performed, and P_{block} was evaluated from the peaks of the "tail" currents. This ensemble protocol is performed for different positive potentials, while the return potential is fixed at −100 mV (Fig. 2C). The voltage-dependence of the steady-state P_{block} at the positive potentials is evaluated for Na^+ (red) and Li^+ (blue) ions (Fig. 2D).

In the case of Li^+ blocking, P_{block} increased monotonously as the membrane potential became more positive, affording a typical sigmoidal shape. The Boltzmann fit was performed for Li^+ blocking, providing a good fit. The electrical distance for the Li^+ blocking was 0.62 ± 0.12 (n = 3 - 26), suggesting that Li^+ reached the selectivity filter by overcoming a high energy barrier. For Na^+ blocking, P_{block} increased as the potential became more positive but remained nearly unchanged at approximately 40% over +200 mV; this value was observed up to +400 mV. This insufficient blocking of Na^+ relative to the full blocking of Li^+ suggests that blocked Na^+ is released from the filter. This phenomenon is reminiscent of the previously reported release of blocked Na^+ to the extracellular space in fast block (13).

Na^+ blocking in the presence of K^+ was examined previously for the KcsA channel (13), and we repeated the experiment (Fig. S3). The single-channel K^+ current at the intracellular K^+ concentration of 180 mM was measured, and the outward current was depressed with the intracellular Na^+ concentration of 20 mM in a voltage-dependent manner. This showed a typical fast blocking of Na^+ at the cavity, but the blocking was alleviated above +200 mV. The relief of fast blocking at high positive potential was called the punchthrough, indicating that the blocked Na^+ was released extracellularly driven by the entering K^+ ions (13). Our repeated experiment reproduced the punchthrough for Na^+ but not for Li^+ (SI Fig. S3A,B).

Similarly, in the case of the slow blocking, the blocked Na^+ is released extracellularly, even in the absence of K^+, as confirmed by single-channel conduction data in the next section (Fig. 3A). The incoming Na^+ ions are pushed out the blocked Na^+, which is hereafter described as a self-punchthrough. The voltage range for the self-punchthrough was similar to that of the punchthrough (Fig. S3C,D), and the voltage-dependency of the slow Na^+ blocking was fitted with a function for the slow blocking model with self-punchthrough (Fig. 2D, Fig. S3C, S10, see Supple. Inf. for details). On the other hand, slow Li^+ blocking was fitted with a Boltzmann function (Fig. 2D). The insufficient blocking of Na^+ relative to the full blocking of Li^+ indicates distinct underlying blocking mechanisms. Li^+ reaches the cavity and, subsequently, the filter, where it stays for ~100 ms until it is released intracellularly upon introducing a negative voltage step (Fig. 2E). In contrast, the incomplete Na^+ blocking suggests that a substantial fraction of the blocked Na^+ is released extracellularly at positive potentials over +250 mV, thus alleviating the slow blocking, by which extracellular K^+ immediately flows in from the beginning of the negative jump (Fig. 2E, broken arrow).

Both punchthrough and self-punchthrough indicate that the selectivity filter allows Na^+ conduction under pushing by either K^+ or Na^+. For Li^+, however, the punchthrough phenomenon was not discernible, indicating that Li^+ was immobilized and remained in the filter even under a large outward driving force.

The single-channel results indicate that at lower positive potentials below +100 mV, Na^+ and Li^+ rarely interfere with the KcsA channel (Fig. 2D), indicating that both Na^+ and Li^+ are mostly excluded from entering the filter. At higher potentials, the distinct behaviors of Na^+ and Li^+ emerge once they entered the filter. Smaller Li^+ binds tightly without conduction, whereas larger Na^+ binds

relatively weaker than Li^+, allowing conduction. As with large K^+ exhibiting a much higher conductance, this size-dependent conductance is a feature of the large-pass filter.

Single-channel Na^+ currents through KcsA channel

To examine Na^+ conduction directly with the single-channel current recordings, which was not possible at the concentration of 200 mM intracellular Na^+, the intracellular Na^+ concentration was increased to 2000 mM (described in Methods). The presence of 100 mM K^+ in the external solution allows evaluation of the number of channels incorporated into the membrane using the inward potassium currents at negative potentials (Fig. 3A). The outward single-channel Na^+ current at +300 mV is successfully recorded in the first direct observation of the single Na^+ current through a selective potassium channel. The single-channel current is 1.2 ± 0.4 pA in amplitude (n = 3) (Fig. 3B; all-point histogram), and the channel exhibits the gating behavior.

Herein, single-channel Na^+ conduction through the wild-type (WT) KcsA channel is also measured (Fig. 3C). In the case of the WT, the channel current was recorded at steady membrane potentials as the open probability is much lower than that of the E71A mutant. Thus, the event-detecting algorithm is applied for the current amplitude of the open state (Fig. 3D; histograms are drawn for the open events; see Methods for details). The single-channel current is 1.02 ± 0.01 pA at +300 mV (n = 3), which is similar to that of the E71A mutant.

As a reference, the single-channel K^+ current was recorded under similar experimental conditions (intracellular K^+ concentration of 2000 mM). The single-channel K^+ amplitude is 94.4 ± 1.8 pA (n = 3) at +300 mV (Fig. 3E), and the conductance (γ) ratio, or γ_{Na}/γ_K value, is 1/78.3. The average residency time of Na^+ in the pore was calculated as ~133 ns from the single-channel current amplitude. Compared to that for K^+ (~1.7 ns), the rate-limiting energy barriers for K^+ and Na^+ permeation differed by 2.6 kcal/mol, thus quantifying the large-pass filter features.

As the single-channel behavior of the E71A mutant at the positive potential is visible, the underlying events of the hitherto invisible slow blocking are discernible. At the positive potential, the Na^+ conducting channel undergoes on-and-off current transitions, and the apparently non-conducting level of the current trace (Fig. 3A) represents the slow blocked state. The blocking probability of ~50% and the closed time of ~100 ms in this current trace corresponds to the P_{block} value and the unblocking time constant deduced from the undetectable blocking, respectively (Fig. 2D and Fig. S2). The opening of the channel from the blocked state at the positive potential indicates that blocked Na^+ was released to the extracellular space under a strong outward driving force, followed by continuous Na^+ flow through the unblocked open channel. The detailed mechanism of the slow blocking is discussed in the SI (Fig. S4 and Fig. S10).

MD simulation of Na^+ permeation through KcsA channel

To understand the conduction process at an atomic scale, the permeation of Na^+ ions through the KcsA channel was examined by employing the MD simulation (31, 44). The WT KcsA channel without the cytoplasmic domain was embedded in a lipid bilayer phosphatidylcholine (PC) membrane (Fig. 4A)(45), and the simulation was performed in either pure K^+ or Na^+ solution with a concentration of 1000 mM. A membrane potential of +350 mV, similar to that of the experiments, was applied, and the outward ion fluxes were examined. Over a simulation time of 4 μs, 137 K^+ ions permeated the KcsA channel, while only four Na^+ ions permeated in 4.5 μs. This value corresponds to the K^+ conductance of 5.5 pA (15.7 pS), which is reasonable in the PC membrane (46). The conductance ratio (γ_{Na}/γ_K) of 38.5 also corresponds to the experimental value (78.3). Recently, Kopec et al. (28) evaluated a current amplitude of 0.46 pA at 220 mV in 300 mM NaCl, and the conductance ratio to K^+ was ~6.7, indicating less selectivity.

The representative trajectories of Na^+ permeation along the z-axis (the pore axis) are shown in Figs. 4B and 4C. As seen in Fig. 4B, two Na^+ ions occupy S3.5–S0.5 (the rational number, such as S3.5, represents the occupancy at the plane site, while the integer number, such as S2, represents the cage site), and Na^+ ions frequently enter the cavity but fail to reach the selectivity filter. Once a Na^+ ion reaches the entrance, Na^+ at S3.5 moves S2 and S1.5 successively. In Fig. 4C, two ions occupy S3.5 (blue) and S1.5 (green) at the beginning, and one ion (red) comes from

the cavity to the entrance site. These three Na^+ ions, moving in concert, reach the S3.5, S2, and S0.5 sites, and the outermost ion (green) left the channel. These sequences of events yield net Na^+ conduction (other trajectories are shown in SI Fig. S5).

Fig. 4D shows the positional distributions of Na^+ (left panel) and K^+ (right panel) ions accumulated along the z-axis over the entire simulation time. The overall distributions along the pore differ substantially for Na^+ and K^+, with more peaks for Na^+ conduction. In the cavity, K^+ is predominantly distributed at the center of the cavity, while Na^+ has an additional site at the entrance of the filter (C-site, Fig. 4D, inset arrow). The integral of probability distribution in the center of the cavity is much higher for K^+ (0.42) than for Na^+ (0.07). This quantity indicates that Na^+ is less accessible to the cavity (13), and the large-pass filter is operative at the cavity, supporting the earlier reports (13, 47).

In the selectivity filter, Na^+ ions are predominantly distributed in the plane sites (S3.5, S1.5, and S0.5), in agreement with the crystal data (35). However, Na^+ ions are also distributed in the cage sites, such as S3 and S2. The ability for Na^+ to occupy either the plane or the cage site in the selectivity filter is referred to as the amphipathic nature of Na^+ binding. Na^+ fluctuates in position frequently between the plane and cage sites (Fig. 4C). Moreover, its amphipathic nature allows varieties of configurations for multiply occupied Na^+ ions in the filter, such as at S3.5-S2-S0.5, and S3-S1.5-S0.

The distribution of Na^+ is further examined using the two-dimensional free energy profile (Fig. 4E). Along the pore, a high energy barrier for Na^+ ions is present between the entrance of the selectivity filter and the S3.5 site. Surprisingly, in the filter, Na^+ ions occupying the cage sites are off-center. This is in contrast to the on-axis occupancy of Na^+ ions in the plane sites and the exclusive on-axis occupancy of K^+ ions throughout the filter. A snapshot reveals that the small Na^+ ion accesses a site near the carbonyl oxygens of the adjacent carbonyl rings of S1.5 and S2.5 and is thus off-center (Fig. 4F). Fig. 4G shows the superimposed locations of the permeating Na^+ and K^+ ions, contrasting off-center Na^+ in the cage sites. The occupancy in the off-center cage sites allows the ready transfer of Na^+ between the cage and plane sites, which opens up a continuous conduit across the selectivity filter. Accordingly, the passage of Na^+ along the selectivity filter is tortuous rather than the straight on-axis pathway for K^+ ions. Moreover, the amphipathic binding to the on-center plane and off-center cage allows multiple Na^+ ions in the filter more degrees of freedom in their configurations.

The amphipathic nature of Na^+ and slow elusion

How is the amphipathic nature of Na^+ related to the conduction? The amphipathic binding of Na^+ yields more numbers of energy wells to be trapped across the filter, which should affect the conductance rate. However, knowing the residency time of each ion in each site is not sufficient to describe conduction and selectivity (9) because, as seen from the MD trajectories (Fig. 4B,C), multiple Na^+ ions participate in conduction. For example, flickery transitions between plane and cage sites are observed (Fig. 4C), which do not yield net conduction. Here, we introduce a previously developed alternative model (31) for characterizing Na^+ conduction.

Various configurations of ions in the filter are categorized into a few states by the number of occupied ions in the filter (discrete random variables, see SI in detail). For example, ion configurations in the plane and cage sites, such as S4-S2.5-S1 and S3.5-S2-S0.5, with three ions in the filter are consolidated into the three-ion occupied state (State 3; Fig. 5C)(22, 31). For the transition from the two-ion occupied state (State 2) to the three-ion occupied state (State 3), an ion is supplied from the cavity side. Then, the outer ion exits to the extracellular space via transitions from State 3 to State 2 via the single-file nature of ion conduction (2, 22). By completing a cyclic transition around State 2 and State 3, a net ion is transferred across the pore (Fig. 5C, Fig. S10).

The MD trajectory at the membrane potential of +1000 mV was obtained for better sampling (Fig. S6 for 1.0 M and Fig. S7 for 0.15 M). 96 Na^+ ions permeated at 1.0 M in the 5.75 μs simulation, and 44 Na^+ ions permeated through the KcsA channel at 0.15 M in the 6 μs simulation time. The patterns of the trajectories were similar to those at +350 mV (Fig. 4B vs. Fig. S6). For example, at 1.0 M, two or three Na^+ ions occupy the selectivity filter, predominantly at S3.5 and

S1.5 sites. At 0.15 M, two Na^+ ions often occupy S3.5 and S1.5 sites, and one ion sometimes is located at S1.5.

The residency times of Na^+ and K^+ for State 1 to State 3 are shown as a distribution (Fig. 5A). The average residency time of State 3 (Fig. 5A upper panel) is very brief (0.16 ns) for K^+ (31), whereas that for Na^+ is prolonged by a factor of about 70 (11.3 ns) relative to that of K^+. This indicates that Na^+ binds to the filter with higher affinity.

The ion flux is expressed by cyclic transitions among States 1 – 3, which is called here 1-2-3 model (Fig. 5C). The coarse-graining of the distinct fine configurations for Na^+ and K^+ as the simple 1-2-3 model allows the quantitative comparison of Na^+ and K^+ conduction. The transition rates (or rate constants) of these states are derived from the residency time and the number of the transitions (Fig. 5B, see Methods)(31), which are shown for Na^+ and K^+ (Fig. 5C). All rate constants for Na^+ are depressed substantially relative to those of K^+. Among them, the transition from State 3 to State 2 for the exit of the outer ion is most prominently depressed. In Fig. 5D, the ratios of the transition rates for Na^+ over K^+ are shown, emphasizing the small value (0.014) for the transition from State 3 to State 2 that is responsible for the slow elution of Na^+.

The results indicate that the selectivity filter structure forms a characteristic space, in which permeating Na^+ and K^+ experience different numbers of binding sites and different types of coordination. The amphipathic nature of Na^+ in binding to either on-center plane or off-center cage site allows the formation of the tortuous path (Fig. 4G), where multiple occupied Na^+ ions have more degrees of freedom in their configurations, rendering entropic contributions to the ion affinity. These ion ensembles participate in collective movements along the filter (Fig. 4B, Fig. S5-7), and the long residency time of the Na^+ ion ensemble yields slow elution (Fig. 5). Accordingly, as a definition of the ion selectivity, the conductance ratio characterizes the large-pass filter via the dynamic nature of the distinct conduction features between Na^+ and K^+, while equilibrium binding suits non-conductive Li^+.

Discussion

In this study, the ion selectivity of the potassium channel is characterized by examining dynamic conduction processes rather than those at equilibrium. The conductance selectivity is adopted as a straightforward measure of the selectivity. To corroborate the use of conductance selectivity, the concept of the band-pass filter is introduced; this illustrates the unusual nature of the potassium channel selectivity, which allows the permeation of ionic species having a limited range of ionic sizes (Fig. 1). The band-pass filter concept permits the deconvolution of the selectivity process into kinetic processes of small- and large-pass filters. The large-pass filter is a prominent feature of the potassium channel, and herein, the kinetic mechanisms underlying the large-pass filter are examined by studying the conduction process across the KcsA potassium channel, as probed using small Na^+ and Li^+ ions (Fig. 2). Examinations of the single-channel current recordings (Fig. 3) as well as atomistic trajectories (Fig. 4,5) elucidate the broad range of the kinetic spectrum of the Na^+ conduction processes in the KcsA channel.

To decompose the conduction processes, the membrane potential provides an avenue for focusing on a specific step of conduction and selectivity. At low positive potential, Na^+ and Li^+ hardly affect the outward K^+ conduction (Fig. 2D, Fig. S3), which characterizes the high energy barrier at the filter entrance. At high positive potential, this barrier is overcome nearly equally for Na^+ and Li^+ (Fig. 2, Fig. S1, S2), indicating the involvement of a dehydration process (1). Henceforth, Na^+ and Li^+ exhibit contrasting behaviors. Distinct single-channel Na^+ conductance is recorded for the first time at a high intracellular Na^+ concentration (2000 mM, Fig. 3A), from which the γ_{Na}/γ_K value of 1/78.3 is obtained. This value is a benchmark for the kinetic characterization of Na^+ conduction. The conductance ratio provides a straightforward expression of the selectivity of the conduction pathway at a given membrane potential as a major driving force, reflecting the integrated permeation processes along the pore. By changing the membrane potential from low to high, critical steps occurring at the cavity, the filter's entrance, and in the filter are gradually shifted and highlighted. We learn that in these multiple steps with distinct selectivity features, the

membrane potential is a crucial factor, thus rationalizing the use of the conductance ratio at a defined potential as a measure of the ion selectivity. In contrast, in the comparison of permeability ratios, the membrane potential is not a major concern.

The MD simulations show a net Na^+ flux across the pore and reproduce the experimentally obtained conductance and its ratio over K^+ with the γ_{Na}/γ_K value of 1/38.5 (Fig. 4), which is comparable to the experimental data. The selectivity filter serves a series of periodic carbonyl oxygen rings (Fig. 6), and permeation is expressed with the 1-2-3 model, in which variable numbers of ion occupancy are allowed (31). At high K^+ concentrations, K^+ ions and water molecules align alternately (K^+-w-K^+-w and w-K^+-w-K^+; where w is a water molecule) (22, 31, 48, 49), which is expressed with the upper cycle (via State 2 and 3) of the 1-2-3 model (Fig. 5C). At low K^+, K^+ permeation via less K^+ occupancy in the filter has been shown (31), representing the lower cycle's contributions. Even at 1 M, the lower cycle is used (Fig. 5A lower panel). Less occupied ions relate to more water molecules in the single-file nature of the selectivity filter, containing up to five permeants; This is in accord with the experimental data of the water-ion coupling ratio towards three (three water molecules and one K^+) (50–52). Recently, a direct knock-on mechanism was proposed (28, 53), in which up to four K^+ ions are condensed in the filter through tight binding of K^+ ions to the cage sites, and knock-on is a prerequisite for permeation. However, this model conflicts with the experimental data of the water-ion coupling ratio (50, 51), which measures the dynamic nature of ion and water permeation rather than equilibrium bindings. The 1-2-3 model covers the permeation process in a wide concentration range by using different cycles and serves as a platform to examine conductance selectivity.

For Na^+, it has been assumed that Na^+ is predominantly located at plane sites rather than the cage sites for K^+ binding (12, 20); herein, the MD simulation demonstrates that Na^+ can bind to either the plane or the cage site (Fig. 4). This is in accordance with our previous observations deduced from the static distribution of ions along the pore (54, 55), indicating that Na^+ binds in an amphipathic (either plane or cage) manner, while Li^+ exclusively binds to the plane sites (12, 54). The gaps between the plane sites lead to poor transfer of Li^+ ions across the filter, reflecting no punchthrough (Fig. 2D). The present simulation reveals that Na^+ ions in the cage sites are located off-center (Fig. 4). Thus, the amphipathic nature of Na^+ binding to the filter is doubled, i.e., plane vs. cage and on-center vs. off-center. These features underpin the tortuous trajectories across the selectivity filter, which provide nearly contiguous pathways for Na^+ passage. Permeating Na^+ ions regard the filter as a tortuous pathway in the long-range, where multiple ions reside. On the other hand, each permeating Na^+ ion is subject to transfer between nearby on-center plane sites and off-center cage sites via the short-range flexibility of the filter.

Doubled binding sites for Na^+ in the filter compared to those for K^+ allows variable occupancy configurations such as "plane–cage–plane" and "on-center–off-center–on-center" (Fig. 4). More degrees of freedom in ion configurations are integrated into the high affinity of Na^+ ion ensembles, which leads to the long residency time: The residency time of State 3 reached 11.3 ns, which is 70 times longer than that of State 3 for K^+ conduction (0.16 ns) (Fig. 5). Accordingly, the tortuosity of the path reconciles the ready conductivity and the high affinity for Na^+ ion ensembles, leading to slow elution. This is the kinetic feature of the conductance selectivity with the large-pass characteristics.

In conclusion, we decomposed the broad spectrum of kinetic phenomena of Na^+ across the pore into multiple critical steps for the conductance selectivity of the potassium channel. The entrance barrier of the selectivity filter provides an initial and effective large-pass filter for dehydration that prefers large K^+ ions over small Na^+ and Li^+ ions (Fig. 2, Fig. SI). Simultaneously, the cut-off radius of 1.7 Å for the filter leads to a small-pass filter for size exclusion. Once ions enter the selectivity filter, the filter structure serves the space for different configurations for each ion species (Fig. 4). The ions are eluted at differential rates, with K^+ exhibiting fast passage, while the flow of small Na^+ ions is retarded (Fig. 3, 5) owing to close interactions with both the plane and cage sites (Fig. 6), and Li^+ remained blocked (Fig. S9). Thus, the barriers at the filter entrance and those in the processes inside the filter constitute an overall large-pass filter. This kinetic differentiation mechanism can be applied to other types of ion channels and served for developing nano-pores with strict selectivity.

From the lessons of the contrasting features of Na^+ and Li^+, we learned that the small conduction of Na^+ through the potassium channel is physiologically meaningful. Once entering the filter by chance, Li^+ is hardly released from the blocked channel except by returning to the cavity, although the channel needs not function for physiologically non-existing Li^+. On the contrary, the substantial conductivity of Na^+ allows the recovery of the channel function. Thus, the high-affinity regime for characterizing the selectivity is relevant to channel blocking. Alternatively, defining the selectivity by differences in conductance is relevant to channel functionality.

Materials and Methods

Sample preparation

The expression, purification, and reconstitution of KcsA channels into liposomes have been previously described (56). Proteoliposomes were prepared by dilution via the following protocol. First, liposomes prepared using azolectin (L-α-phosphatidylcholine type IV-S, Sigma-Aldrich, St. Louis, MO, USA) were suspended in 200 mM KCl at a concentration of 2 mg/mL. Subsequently, an aliquot of the solubilized KcsA channel in 0.06% n-dodecyl-β-D-maltoside (DDM) was diluted 50 times using the liposome solution. The lipid/protein weight ratio of the proteoliposome was 2000. The proteoliposome suspension was mixed with a small amount of concentrated buffer (pH 7.5 or 4.0) just before the experiments. A freshly prepared E71A mutant was used.

Single-channel current recording

Single-channel current recordings were performed using the contact bubble bilayer (CBB) method at room temperature (25℃); the detailed methods have been previously described in the literature (41, 57). Liposome and proteoliposome solutions (2 mg/mL) were filled in two bubble-forming pipettes with tip diameters of approximately 30 μm. The pH of the bubble solutions was asymmetrically set at 7.5 and 4.0; the membrane potential was defined by setting the bubble of pH 7.5 (extracellular side) as the reference side via electrical grounding. The solution was blown from the tip of the pipettes into a hexadecane phase under observation with an inverted microscope (IX73, Olympus, Tokyo, Japan). Small bubbles (diameter of <100 μm) coated with a lipid monolayer were brought into contact through pipette manipulation, forming a CBB. The ionic current was measured using a patch-clamp amplifier (AxoPatch 200B, Molecular Devices, Sunnyvale, CA, USA); data were stored on a personal computer via a low-pass filter (1 kHz cut-off frequency unless otherwise is noted) and an A/D converter (5 kHz sampling; Digidata 1550A, Molecular Devices, Sunnyvale, CA, USA) using the pCLAMP software (Molecular Devices).

The peak of the tail current for the ensemble traces was evaluated by extrapolating the course of time of the blocking recovery to the time of the negative membrane pulse. The voltage-dependent slow blockings of Na^+ and Li^+ were fitted with the function using Mathematica (Wolfram, Il, USA): $P_{block} = 1/(1 + [B]/K_B)$ for Li^+ blocking, where [B] is blocker concentration and $K_B = K_B(0)\ \mathrm{Exp}[-\delta_1 F V/RT]$ (δ_1: electric distance, F: the Faraday constant, R: the Gas constant, T: the absolute temperature, V: the membrane potential, $K_B(0)$: equilibrium dissociation constant of the blocker). For Na^+ blocking, the blocking model and the fitted parameters are shown in SI (Fig. S10).

For recordings in the 2000 mM Na^+ solution, a similar pulse protocol was used for the E71A mutant, and the all-point histogram was drawn for the single-channel conductance. For the WT channel with its low open probability, the single-channel current was recorded in the steady-state membrane potential. The open time was very brief, and the single-channel events were detected using the event-detecting algorithm implemented in the program QuB (58). Accordingly, the histogram was drawn exclusively for the open state rather than both open and closed states.

Molecular dynamics simulations

MD simulations were performed on the transmembrane domain of the KcsA potassium channel, which was embedded in a PC membrane and bathed in a solution of 1 M NaCl. The following empirical potentials were used: the TIP3P model for water, ff94 force field for the channel, and

those developed by Smith and Dang (59) for Na^+. Other detailed simulation conditions have been described in Supplementary Materials (31, 45). Positive membrane potentials of +350 mV or +1000 mV were applied, and the outward Na^+ flux was examined. Our previous study showed that the root-mean-square fluctuation of the α-carbon atoms in the transmembrane domain was < 2.0 Å (45), indicating that the channel remained in an open conformation throughout the simulation.

MD simulations were performed using the AMBER11 package (60). To minimize the dependence of the trajectories on the initial coordinates, fifty different initial coordinates were generated for both the open structures at the NVT ensemble (310 K). A periodic boundary condition was imposed. Electrostatic interactions were calculated using the particle mesh Ewald method (61) with a 0.8-nm cutoff in real space. The cutoff of the Lennard–Jones interaction was 0.8 nm. The bonds including those of H atoms were constrained using the SHAKE algorithm (62), enabling a time step of 2 fs.

Transition rates

The transition rates were derived from the residency time and the number of the transitions (31). The residency time of State 2 (τ_2), for example, is related to the rate constants exiting from the State 2 such as the rate from State 2 to State 3 (k_{23}) and State 2 to State 1 (k_{21}) as well as the relative preference to the transitions. Thus,

$$\tau_2 = 1/(k_{21} + k_{23}) = 1/(k_{21} + N_{23}/N_{21})$$

where N_{21} and N_{23} are the observed number of transitions from State 2 → State 1 and State 2 → State 3, respectively, in which $N_{23}/N_{21} = k_{23}/k_{21}$ is used. Accordingly, the transition rates of k_{23} and k_{21} are obtained by counting N_{23}/N_{21}.

Acknowledgments

We thank Dr. Andy James (University of Bristol) and Dr. Hidehiko Okazawa (University of Fukui) for discussions and Editage for providing English language editing.

References

Paste your main manuscript references here. They should be listed in order of citation.

1. Hille B (2001) *Ion channels of excitable membranes* (Sinauer Associates Inc, Sunderland). 3rd Ed.
2. Hodgkin AL, Keynes RD (1955) The potassium permeability of a giant nerve fibre. *J Physiol* 128:61–88.
3. Bezanilla F, Armstrong CM (1972) Negative conductance caused by entry of sodium and cesium ions into the potassium channels of squid axons. *The Journal of general physiology* 60:588–608.
4. Eisenman G, Horn R (1983) Ionic selectivity revisited: The role of kinetic and equilibrium processes in ion permeation through channels. *The Journal of Membrane Biology* 76(3):197–225.
5. Nonner W, Chen DP, Eisenberg B (1999) Progress and Prospects in Permeation. *The Journal of General Physiology* 113(6):773–782.
6. Andersen OS (2011) Perspectives on: Ion selectivity. *The Journal of general physiology* 137(5):393–5.
7. Heginbotham L, Lu Z, Abramson T, MacKinnon R (1994) Mutations in the K^+ channel signature sequence. *Biophysical journal* 66(4):1061–7.

8. Derebe MG, et al. (2011) Tuning the ion selectivity of tetrameric cation channels by changing the number of ion binding sites. *Proceedings of the National Academy of Sciences of the United States of America* 108(2):598–602.
9. Flood E, Boiteux C, Lev B, Vorobyov I, Allen TW (2019) Atomistic Simulations of Membrane Ion Channel Conduction, Gating, and Modulation. *Chemical Reviews* 119(13):7737–7832.
10. Nogueira JJ, Corry B (2018) *Ion Channel Permeation and Selectivity* (Oxford University Press, Oxford). Oxford Han doi:10.1093/oxfordhb/9780190669164.013.22.
11. Lockless SW (2015) Determinants of cation transport selectivity: Equilibrium binding and transport kinetics. *Journal of General Physiology* 146(1):3–13.
12. Thompson AN, et al. (2009) Mechanism of potassium-channel selectivity revealed by Na^+ and Li^+ binding sites within the KcsA pore. *Nature structural & molecular biology* 16(12):1317–24.
13. Nimigean CM, Miller C (2002) Na^+ Block and Permeation in a K^+ Channel of Known Structure. *The Journal of General Physiology* 120(3):323–335.
14. Noskov SY, Bernèche S, Roux B (2004) Control of ion selectivity in potassium channels by electrostatic and dynamic properties of carbonyl ligands. *Nature* 431:830–834.
15. Furini S, Domene C (2011) Selectivity and permeation of alkali metal ions in K^+-channels. *Journal of molecular biology* 409(5):867–78.
16. Sauer DB, Zeng W, Canty J, Lam Y, Jiang Y (2013) Sodium and potassium competition in potassium-selective and non-selective channels. *Nature communications* 4(May):2721.
17. Nematian-Ardestani E, Jarerattanachat V, Aryal P, Sansom MSP, Tucker SJ (2017) The effects of stretch activation on ionic selectivity of the TREK-2 K2P K^+ channel. *Channels* 11(5):1–5.
18. Doyle DA, et al. (1998) The structure of the potassium channel: Molecular basis of K^+ conduction and selectivity. *Science* 280(5360):69–77.
19. Yu H, Yu. Noskovb S, Roux B (2010) Two mechanisms of ion selectivity in protein binding sites. *Proceedings of the National Academy of Sciences of the United States of America* 107(47):20329–20334.
20. Kim I, Allen TW (2011) On the selective ion binding hypothesis for potassium channels. *Proceedings of the National Academy of Sciences of the United States of America* 108(44):17963–8.
21. Shrivastava IH, Peter Tieleman D, Biggin PC, Sansom MSP (2002) K^+ versus Na^+ Ions in a K Channel Selectivity Filter: A Simulation Study. *Biophysical Journal* 83(2):633–645.
22. Morais-Cabral JHH, Zhou Y, MacKinnon R (2001) Energetic optimization of ion conduction rate by the K^+ selectivity filter. *Nature* 414(6859):37–42.
23. DeMarco KR, Bekker S, Vorobyov I (2018) Challenges and advances in atomistic simulations of potassium and sodium Ion channel gating and permeation. *The Journal of Physiology* 0:1–20.
24. Zhou Y, Morais-Cabral JH, Kaufman A, Mackinnon R (2001) Chemistry of ion coordination and hydration revealed by a K^+ channel-Fab complex at 2.0 Å resolution. *Nature* 414(6859):43–48.
25. Lockless SW, Zhou M, MacKinnon R (2007) Structural and thermodynamic properties of selective ion binding in a K^+ channel. *PLoS biology* 5(5):e121.
26. Renart ML, et al. (2017) Selective exclusion and selective binding both contribute to ion selectivity in KcsA, a model potassium channel. *Journal of Biological Chemistry* 292(37):15552–15560.
27. Zhou Y, MacKinnon R (2003) The Occupancy of Ions in the K^+ Selectivity Filter: Charge Balance and Coupling of Ion Binding to a Protein Conformational Change Underlie High Conduction Rates. *Journal of Molecular Biology* 333(5):965–975.
28. Kopec W, et al. (2018) Direct knock-on of desolvated ions governs strict ion selectivity in K^+ channels. *Nature Chemistry* 10(8):813–820.
29. Liu S, Lockless SW (2013) Equilibrium selectivity alone does not create K^+-selective ion conduction in K^+ channels. *Nature Communications* 4:1–7.

30. Furutani Y, Shimizu H, Asai Y, Oiki S, Kandori H (2015) Specific interactions between alkali metal cations and the KcsA channel studied using ATR-FTIR spectroscopy. *Biophysics and Physicobiology* 12:37–45.
31. Sumikama T, Oiki S (2019) Queueing arrival and release mechanism for K^+ permeation through a potassium channel. *J Physiol Sci* 69:919–930.
32. Sun Z, Xu Y, Zhang D, McDermott AE (2019) Probing Allosteric Coupling of a Constitutively Open Mutant of the Ion Channel KcsA using Solid State NMR. *Proc Natl Acad Sci USA* 117(13):7171–7175.
33. Roux B (2017) Ion channels and ion selectivity. *Essays in Biochemistry* 61(2):201–209.
34. Dudev T, Lim C (2009) Determinants of K^+ vs Na^+ selectivity in potassium channels. *Journal of the American Chemical Society* 131(23):8092–8101.
35. Nimigean CM, Allen TW (2011) Origins of ion selectivity in potassium channels from the perspective of channel block. *Journal of General Physiology* 137(5):405–413.
36. Thomas M, Jayatilaka D, Corry B (2011) Mapping the importance of four factors in creating monovalent ion selectivity in biological molecules. *Biophysical Journal* 100(1):60–69.
37. Klesse G, Rao S, Tucker SJ, Sansom MSP (2020) Induced Polarization in Molecular Dynamics Simulations of the 5-HT 3 Receptor Channel. *Journal of the American Chemical Society* 142(20):9415–9427.
38. Sakmann B, Neher E (2009) *Single-Channel Recording* (Springer, New York). 2nd Ed.
39. Hille B (1973) Potassium Channels in Myelinated Nerve: Selective permeability to small cations. *The Journal of General Physiology* 61(6):669–686.
40. Schultz SG (1980) *Basic Principles of Membrane Transport* (Cambridge University Press, London).
41. Iwamoto M, Oiki S (2015) Contact Bubble Bilayers with Flush Drainage. *Scientific Reports* 5:9110.
42. Oiki S, Iwamoto M (2018) Lipid bilayers manipulated through monolayer technologies for studies of channel-membrane interplay. *Biological and Pharmaceutical Bulletin* 41(3). doi:10.1248/bpb.b17-00708.
43. Iwamoto M, Oiki S (2018) Constitutive boost of a K^+ channel via inherent bilayer tension and a unique tension-dependent modality. *Proceedings of the National Academy of Sciences of the United States of America* 115(51):13117–13122.
44. Sumikama T, Oiki S (2016) Digitalized K^+ Occupancy in the Nanocavity Holds and Releases Queues of K^+ in a Channel. *Journal of the American Chemical Society* 138(32):10284–10292.
45. Sumino A, Sumikama T, Iwamoto M, Dewa T, Oiki S (2013) The Open Gate Structure of the Membrane-Embedded KcsA Potassium Channel Viewed From the Cytoplasmic Side. *Scientific reports* 3:1063.
46. Iwamoto M, Oiki S (2013) Amphipathic antenna of an inward rectifier K^+ channel responds to changes in the inner membrane leaflet. *Proceedings of the National Academy of Sciences of the United States of America* 110(2):749–54.
47. Zhou Y, MacKinnon R (2004) Ion Binding Affinity in the Cavity of the KcsA Potassium Channel. *Biochemistry* 43(17):4978–4982.
48. Tilegenova C, et al. (2019) Structure, function, and ion-binding properties of a K^+ channel stabilized in the 2,4-ion–bound configuration . *Proceedings of the National Academy of Sciences* 116(34):16829–16834.
49. Kratochvil HT, et al. (2016) Instantaneous ion configurations in the K^+ ion channel selectivity filter revealed by 2D IR spectroscopy. *Science* 353(6303):1040–1044.
50. Ando H, Kuno M, Shimizu H, Muramatsu I, Oiki S (2005) Coupled K^+-water flux through the HERG potassium channel measured by an osmotic pulse method. *The Journal of general physiology* 126(5):529–38.
51. Iwamoto M, Oiki S (2011) Counting Ion and Water Molecules in a Streaming File through the Open-Filter Structure of the K Channel. *The Journal of neuroscience* 31(34):12180–8.

52. Chang HK, Iwamoto M, Oiki S, Shieh RC (2015) Mechanism for attenuated outward conductance induced by mutations in the cytoplasmic pore of Kir2.1 channels. *Sci Rep* 5:18404.
53. Köpfer DA, et al. (2014) Ion permeation in K^+ channels occurs by direct Coulomb knock-on. *Science* 346:352–355.
54. Phongphanphanee S, Yoshida N, Oiki S, Hirata F (2014) The “ambivalent” snug-fit sites in the KcsA potassium channel probed by “3D-RISM microscopy.” *Pure and Applied Chemistry* 86(2):97–104.
55. Phongphanphanee S, Yoshida N, Oiki S, Hirata F (2014) Distinct configurations of cations and water in the selectivity filter of the KcsA potassium channel probed by 3D-RISM theory. *Journal of Molecular Liquids* 200:52–58.
56. Iwamoto M, et al. (2006) Surface structure and its dynamic rearrangements of the KcsA potassium channel upon gating and tetrabutylammonium blocking. *The Journal of biological chemistry* 281(38):28379–86.
57. Iwamoto M, Oiki S (2018) Lipid Bilayer Experiments with Contact Bubble Bilayers for Patch-Clampers. *Journal of Visualized Experiments* (January):1–11.
58. Nicolai C, Sachs F (2013) Solving Ion Channel Kinetics with the QuB Software. *Biophysical Reviews and Letters* 08(03):1–21.
59. Smith DE, Dang LX (1994) Computer simulations of NaCl association in polarizable water. *Journal of Chemical Physics* 100:3757.
60. Case DA, Darden TA, Cheatham III TE, Al. E (2010) *AMBER 11*.
61. Essmann U, Perera L, Berkowitz M (1995) A smooth particle mesh Ewald method. *The Journal of chemical physics* 103(November):31–34.
62. Ryckaert J, Ciccotti G, Berendsen HJC (1977) Numerical integration of the cartesian equations of motion of a system with constraints: molecular dynamics of n-alkanes. *Journal of Computational Physics* 23(3):327–341.

Figures and Tables

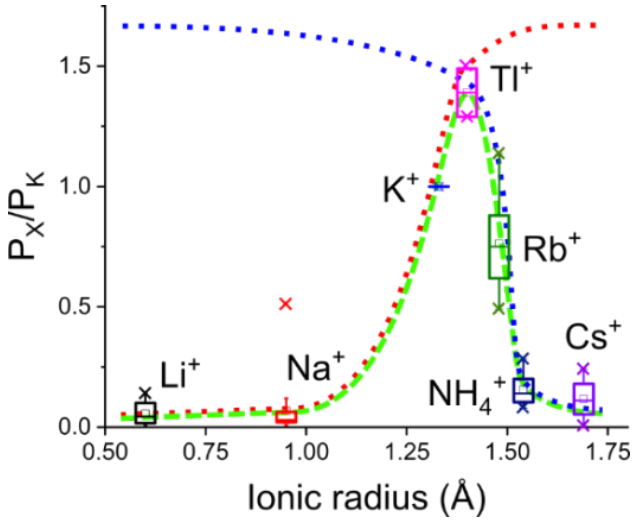

Figure 1. Ion selectivity of potassium channels. Permeability ratios of monovalent cations relative to K^+ as a function of ionic radius are shown for various types of potassium channels. The data were collected from the literature (see SI Tab. S1) and were drawn as a box plot, where the box covers the 25th to 75th percentiles with the center line indicating the median. The "whisker" from the box indicates 1.5 times quartile, and outliers are shown as crosses. The potassium channel selectivity is characterized as a band-pass filter with a limited ion-size window (broken green line). The band pass is arbitrarily decomposed into plausible small-pass (or low-pass; broken blue line) and large-pass (or high-pass; broken red line) filters. The lines do not have physical meanings.

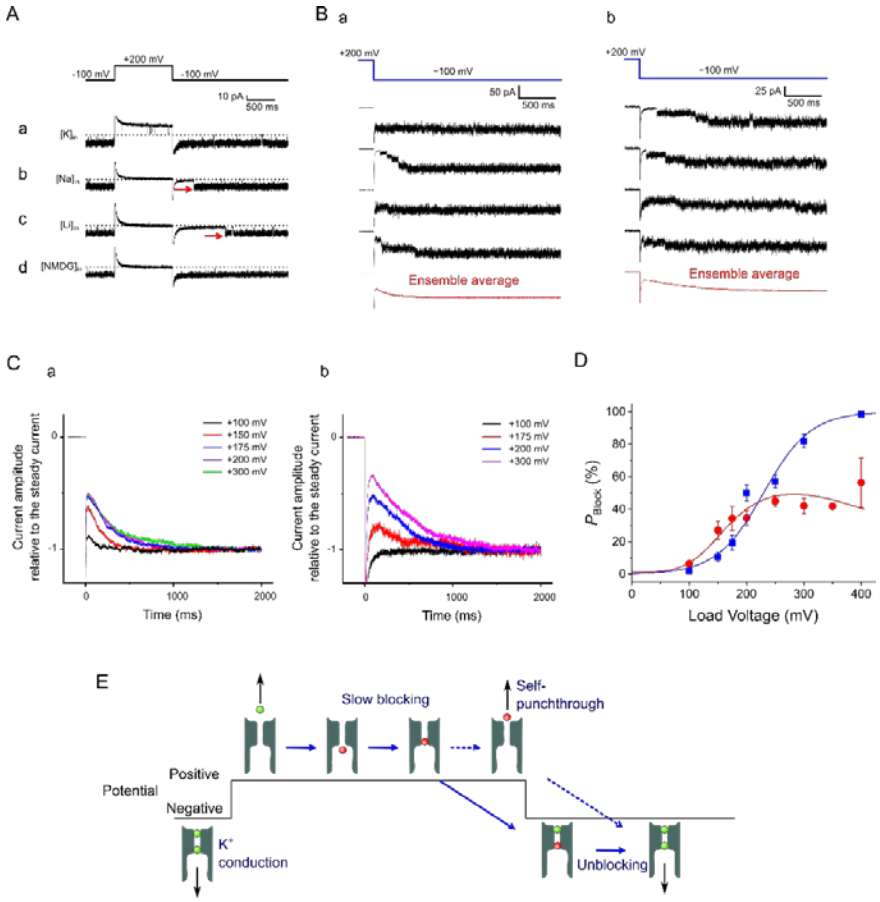

Figure 2. Voltage-dependent blocking by Na^+ and Li^+. A. Single-channel current recordings from the E71A mutant of KcsA channel in different intracellular cationic solutions. The single-channel currents are measured using a pulse protocol (+200 mV) of 1-s duration followed by a negative potential (−100 mV; holding potential was −100 mV). The extracellular solution contained 200 mM KCl, and the intracellular solution contained 200 mM of K^+ (a), Na^+ (b), Li^+ (c), and $NMDG^+$ (d). In the symmetric K^+ solution (a), signature E71A currents are recorded, such as the single-channel current amplitude of 17.7 pA at a positive potential, flickering currents at the negative potential, and the open probability of almost 100% at both −100 mV and +200 mV. **B.** Delayed openings at negative potentials in Na^+ (a) and Li^+ (b) solutions. A repeated pulse protocol similar to that mentioned in A is applied to the membrane containing a few channels, and the representative current traces are shown. The ensemble current trace (red) obtained from 100 raw traces is shown. **C.** Voltage-dependent blocking for Na^+ (a) and Li^+ (b). The ensemble current traces for different positive potentials for Na^+ (a) and Li^+ (b) are shown. **D.** Steady-state blocking probability (P_{block}) of the channel by Na^+ (red) or Li^+ (blue) ions as a function of the membrane potential. P_{block} is evaluated as the instantaneous current level at the negative potential relative to the steady-state current amplitude. The error bars represent SEM (n = 3 – 30 for Na^+ and 3 – 26 for Li^+). The data are fitted with the function (see Methods) with the parameters z = 0.62 ± 0.12 for Li^+. For Na^+, the blocking model and fitted parameters are shown in SI (Fig. S10). **E.** Schematic for the slow Na^+ (red) blocking. The channel remains either blocked or unblocked at positive potentials, and unblocking occurs by self-punchthrough (broken arrow). Upon a negative jump, the blocked channel is unblocked, leading to a delayed opening with inward K^+ (green) conduction. The unblocked channel allows inward K^+ conduction from the beginning of the negative jump.

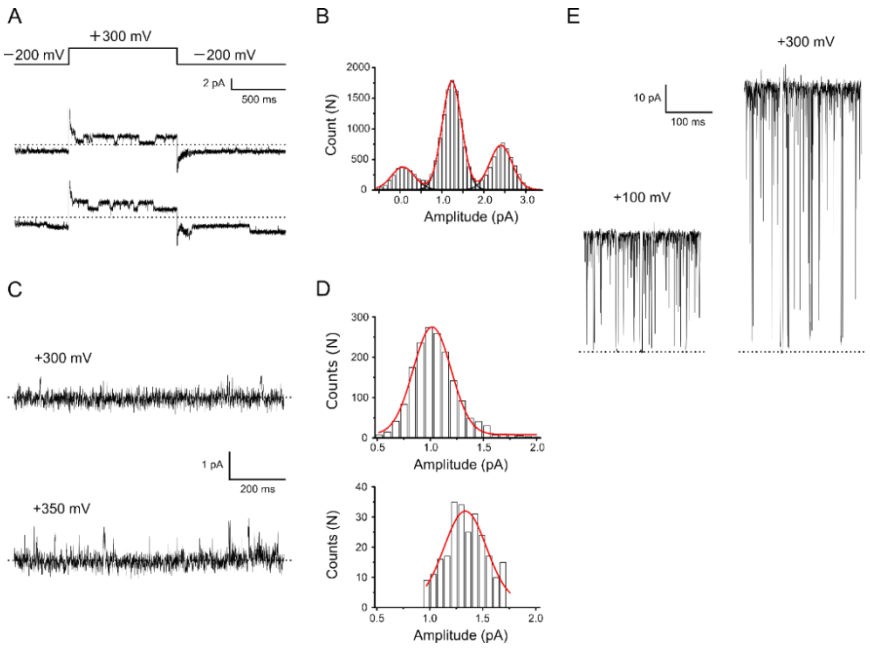

Figure 3. Single-channel Na^+ currents of the KcsA channel. A. Representative Na^+ current traces of E71A mutant with a positive pulse of +300 mV (2 M NaCl intracellular solution and 0.1 M KCl with 1.9 M $Tris^+$ extracellular solution). The currents were low-pass filtered at 800 Hz. **B.** Single-channel current histogram at +300 mV (all-points amplitude histogram). The membrane contains two channels, and the histogram is fitted with a binomial distribution, which gives an open probability of ~50%. The single-channel current amplitude was 1.2 ± 0.4 (n = 3) at +300 mV. **C.** Representative single-channel current traces of the wild-type (WT) channel at +300 (upper) and +350 mV (lower). The dashed line represents the zero-current level. The same solutions as those for the E71A experiments were used. The currents were low-pass filtered at 800 Hz. **D.** Single-channel current amplitude of the WT channel at +300 mV (upper) and +350 mV (lower). For the low-open probability channel, rare opening events are detected with an event-detecting algorithm [44], in which the amplitudes of current jumps upon openings are accumulated for the histogram. The single-channel current amplitude is 1.02 ± 0.01 (n = 3) at +300 mV and 1.33 ± 0.02 pA (n = 3) at +350 mV. **E.** Representative single-channel K^+ current traces of E71A mutant. These are recorded in a symmetric 2 M KCl solution at +100 and +300 mV. The single-channel current amplitude is 41.9 ± 1.1 (n = 3) at +100 mV and 94.4 ± 1.8 pA (n = 3) at +300 mV. The dashed line represents the zero-current level.

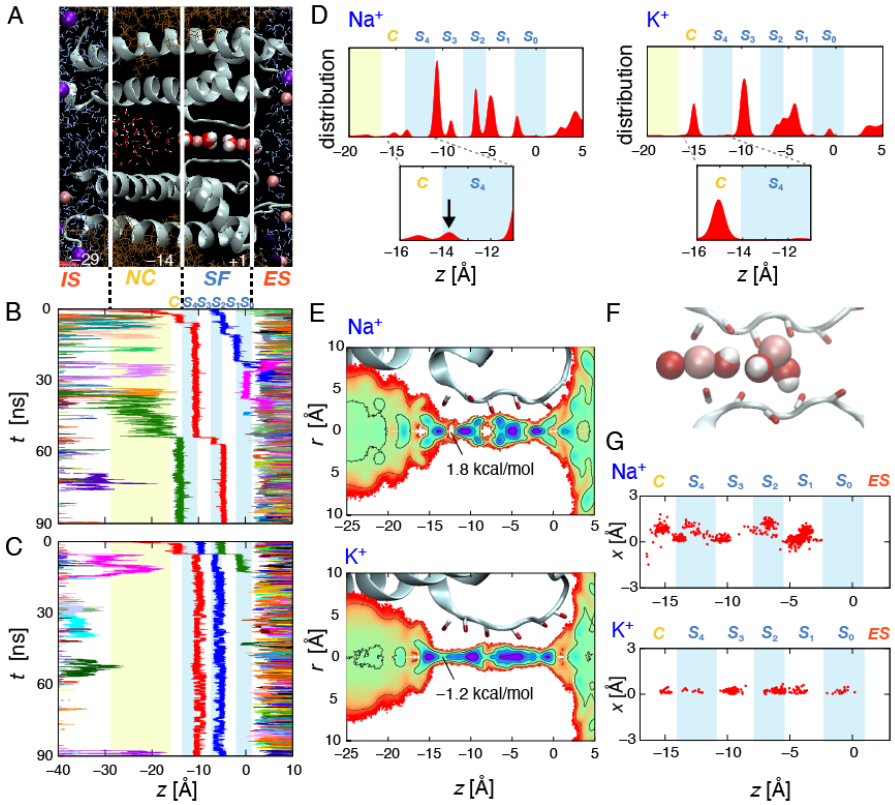

Figure 4. MD simulation of Na^+ permeation through the KcsA channel. A. KcsA channel embedded in the PC membrane. The names of the permeation pathway are as follows. IS: intracellular space, NC: (nono-)cavity, SF: selectivity filter, and ES: extracellular space. The site in the NC that is closest to the filter is termed as the C site. Light red spheres correspond to Na^+, purple spheres indicate Cl-, and red and white spheres indicate water molecules. **B.** Representative Na^+ trajectory. The time course of the position of Na^+ ions along the z-axis (z = 0 at the S0 site) is shown. Each color represents an individual trajectory of Na^+. The light blue and white stripes are bound by the carbonyl oxygens of the filter backbone; these are the five cage sites for K^+ binding, named S0–S4. Na^+ enters the NC frequently but returns to the IS. In the SF, Na^+ ions occupy at either plane or cage sites. The Na^+ concentration was 1 M, and the membrane potential was +350 mV. **C.** Additional trajectory involves three Na^+ ions moving in concert. **D.** Distribution of Na^+ and K^+ ions across the pore. In the cavity, Na^+ ions are distributed at the entrance of the filter (C-site, arrow), wherein the K^+ ions are not occupied (inset). In the filter, Na^+ ions are distributed either in the cage (represented with integer numbers such as S2) or plane (represented with real numbers such as S3.5) sites, while K^+ ions are mostly distributed at the cage sites. **E.** 2D distribution of Na^+ and K^+ in the selectivity filter. Two-dimensional (z – r axis) free energy distribution of K^+ (upper) and Na^+ (lower) around the selectivity filter. Each contour line corresponds to the free energy difference of 1 kcal/mol. The box size is 1.5 Å-1. At the cage site, the Na^+ distribution is split into two peaks away from the central axis, whereas the K^+ distribution remains centered across the filter. **F.** Snapshot of Na^+ ions in the filter. Two Na^+ ions occupy S3.5 and S0.5. The on-centered Na^+ in the S3.5 plane site (left) is flanked by two water molecules. The off-center Na^+ in the S2 cage site (right) is solvated by the carbonyl oxygens of two adjacent rings as well as by water molecules. **G.** Superimposed locations of permeating Na^+ and K^+ ions in 2D coordinates of the filter.

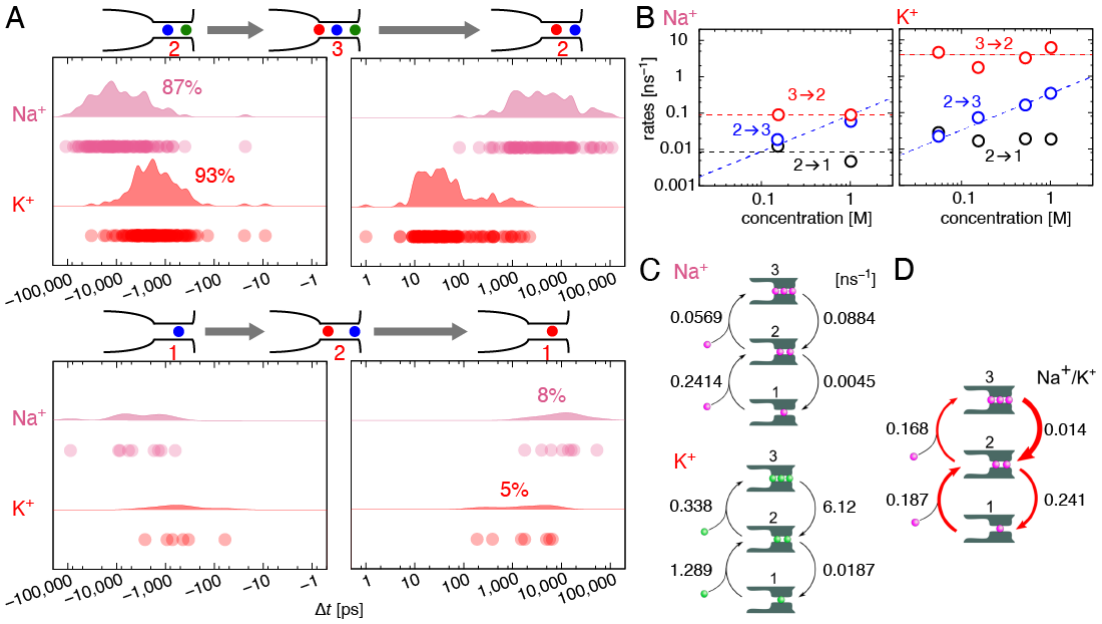

Figure 5. Conductance rates of Na^+ and K^+ through the KcsA channel. A. The residency time of each ion-occupied state. Up to three ions can occupy the filter (States 1-3). The net ion flux occurs through transitions between less-ion occupied states and more-ion occupied states, such as State 2- State 3 (upper panel): State 2 transitions to State 3 as an ion enters the filter from the cavity. Subsequently, as an outer ion exits towards the extracellular space, State 3 returns to State2. Completing a cycle yields a net ion flux across the channel. The residency time of each ion-occupied state sampled from the MD simulation data is expressed as dots (raw data), and the distributions of the residency time are shown based on kernel density estimations [29,63]. In this condition (1 M, +1000 mV), conduction occurs predominantly through transitions between State 2 and 3 for both Na^+ and K^+. The residency time of State 3 for Na^+ is prolonged 100 times relative to that for K^+, which is responsible for the slow elution of Na^+. **B.** Concentration dependency of the rate for Na^+ and K^+ conduction. The transition rates of these states are derived from the residency time and the number of the transitions (see Methods). The rates from State 2 to State 1 (red) and State 3 (black) are shown. The blue dashed line represents a linear fit for the data (rate = $[K^+] \cdot 0.33$ ns−1), and the red dashed line is a fit calculated from a constant (3.89 ns−1). For Na^+, the blue dashed line represents the rate = $[Na^+] \cdot 0.088$ ns-1, and the red dashed line is a constant of 0.091 ns-1. **C.** The simple permeation models for Na^+ and K^+ conduction involving State 1 – 3 (1-2-3 model) at 1.0 M [29]. The continuous ion permeation process is expressed with a set of the occupied ion numbers (discrete random variables), and the probability and transitions among them yield the net ion flux (see Supple. Inf.)[64,65]. The transition rates between states for Na^+ are deduced from B. **D.** Comparison of the rates for Na^+ and K^+. The thickness of the arrows (red) represents the relative rates of Na^+ in respect of K^+, with the thicker ones indicating more attenuation. All rates are depressed for the Na^+ conduction, but the rate State 3→2 is the most prominently depressed, leading to the low Na^+ conductance.

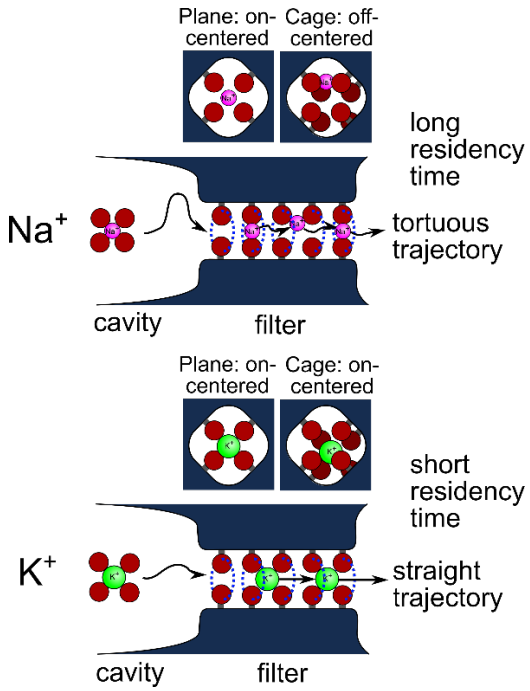

Figure 6. Distinct conductance features of Na^+ and K^+ through KcsA channel filter via the large-pass filter. The mechanism for the large-pass filter favoring large K^+ ions over small Na^+ ions is shown. A schematic of Na^+ (top) and K^+ (bottom) in the cavity (left; fully hydrated) and the selectivity filter (right, upper left: cross-sectional view of the plane site, upper right: cross-sectional view of the cage site, lower: longitudinal view). The dark red spheres represent the oxygen atoms of the water molecules (in the cavity), carbonyl, or hydroxyl groups of threonine (in the filter), and the darker red spheres in the right upper panels indicate oxygen atoms in an adjacent ring. Upon entering the filter, a much higher dehydration energy barrier is imposed for Na^+, as deduced from the fast and slow blockings. In the filter, K^+ is centered, while Na^+ is off-center in the cage sites and centered in the plane sites, leading to tortuous trajectories for Na^+. An off-center Na^+ interacts with the carbonyl oxygens of the adjacent rings (right upper panel), whereas a centered Na^+ interacts with the carbonyl oxygens of a ring (plane site). These affinities to multiple sites are integrated into the longer residency time of multiple Na^+ ions in the filter, leading to slow elution (Fig. 5).